iScience

CellPress
OPEN ACCESS

Article

Alterations in histology of the aging salivary gland and correlation with the glandular inflammatory microenvironment

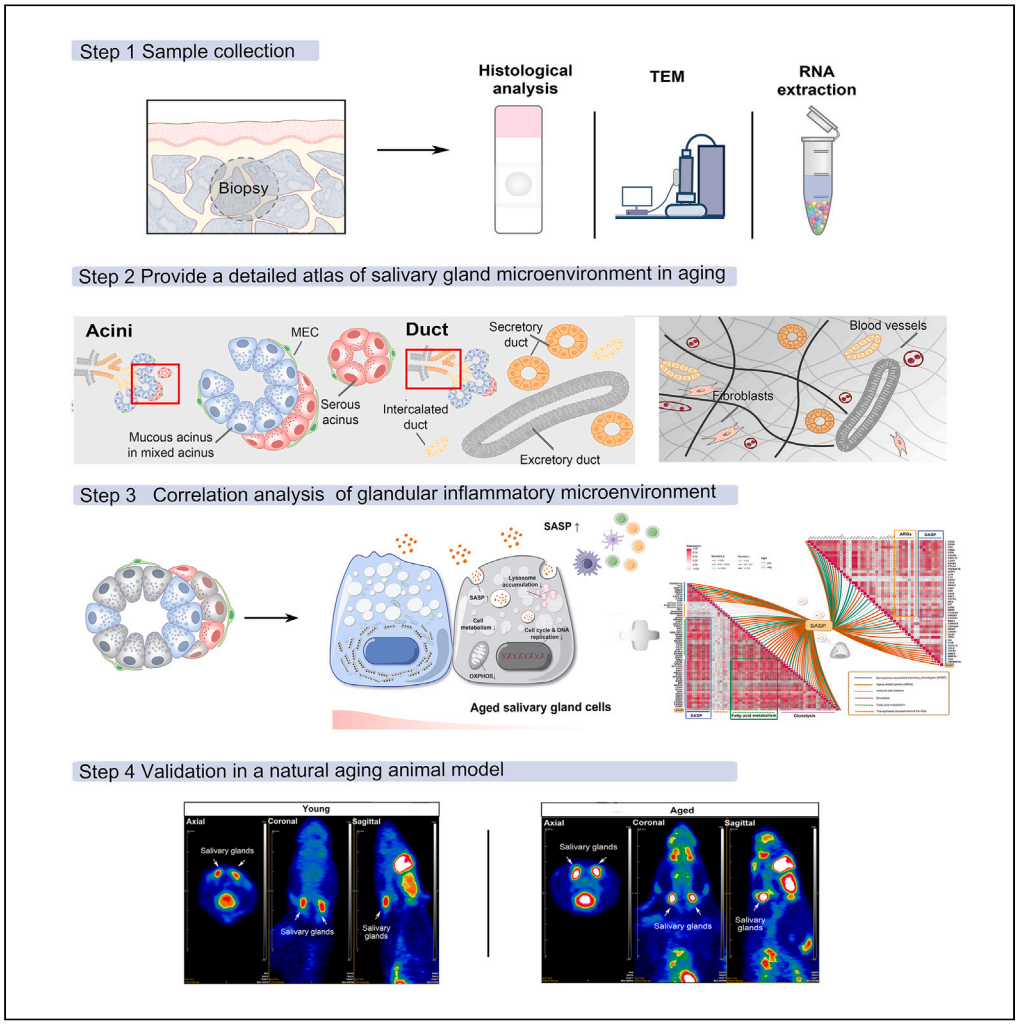

Ning Li, Yulin Ye, Yicheng Wu, ..., Wangxi Hai, Yinyin Xie, Liting Jiang

wangxi.hai@sjtu.edu.cn (W.H.)
yyin_xie@163.com (Y.X.)
drjiangliting@163.com (L.J.)

Highlights

Generated a histological atlas of young and aged human minor salivary glands

Lysosomes and autophagolysosomes accumulated in aged acinar and ductal cells

SASP genes were highly correlated with the aging salivary gland microenvironment

OXPHOS impairment occurs in salivary glands of natural aging rats

Li et al., iScience 26, 106571
May 19, 2023
https://doi.org/10.1016/j.isci.2023.106571

iScience

CellPress
OPEN ACCESS

Article

Alterations in histology of the aging salivary gland and correlation with the glandular inflammatory microenvironment

Ning Li,[1,6] Yulin Ye,[1,6] Yicheng Wu,[2,6] Lei Li,[3,6] Jiawei Hu,[1] Danyang Luo,[1] Yusi Li,[1] Jie Yang,[2] Yiming Gao,[1] Wangxi Hai,[4,*] Yinyin Xie,[5,*] and Liting Jiang[1,7,*]

SUMMARY

Aging-related salivary dysfunction typically causes reduced saliva volumes, which leads to debilitating consequences, even affecting patient quality of life. Understanding the respective clinicopathological characteristics and molecular mechanisms underlying salivary gland functioning during aging is vital for therapeutic purposes. Here, we provide a detailed atlas of the salivary gland microenvironment during aging, and we identified several phenotypes characteristic of aging salivary glands, including acini atrophy, increased inflammatory cells, altered immune responses, and accumulation of lysosomes and autophagosomes in aging cells, which may reflect progressive degeneration of salivary gland function. Furthermore, our analyses suggested significant enrichment of metabolic pathways in aging glands. Our results revealed complex cellular cross-talk among aging acinar cells, inflammatory factors, and immune responses. A natural aging animal model was established to verify these findings. This study provides mechanistic insights into age-related clinicopathogenesis, important implications for early diagnosis, and identification of new targets for improving salivary gland dysfunction.

INTRODUCTION

Aging is the gradual and irreversible decline in physiological function that affects almost all tissues of organisms,[1] including the salivary glands which are significantly affected. Many studies confirmed degenerative alterations in the histological structure of salivary glands and changes in the saliva volume and components with age. Saliva is mainly produced by acinar cells; thus, age-related salivary dysfunction typically causes reduced saliva volumes, which lead to debilitating consequences, including increased susceptibility to dental caries and oral infections and swallowing difficulties, which affect the quality of life.[2,3] To date, there is no permanent or definitive therapeutic approach to resolve the irreversible impairment of the salivary glands. Therefore, understanding the clinicopathological features and molecular mechanisms that control salivary gland function during aging is highly relevant for therapeutic purposes.

As humans age, the fibro-adipose tissue increases while the number of acini decreases.[2] The specific cellular and molecular mechanisms leading to such aging-related dysfunction process are only beginning to be understood. A widely held view is that stem cells, within larger excretory and striated ducts, and progenitor cells, within the striated and intercalated ducts, can self-renew and differentiate. Once acinar cells are damaged, replacement occurs through stem/progenitor cell differentiation.[4] In the salivary glands of aged mice, a decline in the stem cell number and proliferative activity of cluster differentiation marker (CD) 133+ stem/progenitor cells was observed.[5] Tissue-resident stem/progenitor cells can restore the impaired gland structure and function and continuously replenish aged saliva-producing cells. A recent study identified a combined marker, the intraflagellar transport protein 140 (IFT140) and keratin-14, for salivary gland stem/progenitor cells.[6] The authors elucidated IFT140 was essential for regulating salivary stem/progenitor cell differentiation and gland regeneration. In contrast, another study combining genetic pulse-chase experiments with single-cell clonal analyses and lineage-tracing analyses has shown that salivary gland homeostasis is maintained through acinar cell self-renewal by self-duplicating without a significant input from stem/progenitor cells.[7,8] Whether stem cell dysfunction in the salivary glands is directly

[1]Department of Stomatology, Ruijin Hospital, Shanghai Jiao Tong University School of Medicine, College of Stomatology, Shanghai Jiao Tong University, Shanghai, China

[2]Core Facility of Basic Medical Sciences, Shanghai Jiao Tong University, School of Medicine, Shanghai, China

[3]Department of Pathology, Ruijin Hospital, Shanghai Jiao Tong University School of Medicine, Shanghai, China

[4]Department of Nuclear Medicine, Ruijin Hospital, Shanghai Jiao Tong University School of Medicine, Shanghai, China

[5]Shanghai Institute of Hematology, State Key Laboratory of Medical Genomics, National Research Center for Translational Medicine at Shanghai, Ruijin Hospital, Shanghai Jiao Tong University School of Medicine, Shanghai, China

[6]These authors contributed equally

[7]Lead contact

*Correspondence: wangxi.hai@sjtu.edu.cn (W.H.), yyin_xie@163.com (Y.X.), drjiangliting@163.com (L.J.)

https://doi.org/10.1016/j.isci.2023.106571

associated with histological changes in the salivary glands during aging should be further elucidated. Salivary glands mainly consist of secretory acinar cells and ductal cells;[7] we thus examined how these functional cells responded to aging.

A landmark paper in 2013 identified and categorized nine hallmarks of aging.[1] One fundamental aging mechanism that underlies numerous age-related diseases is cellular senescence. In young organisms, cellular senescence represents an important barrier against cellular transformation and prevents the uncontrolled proliferation of cells that are relevant for cancer and aging. Due to inefficient turnover system, these senescent cells may accumulate in aged tissues and contribute to age-related pathology. The elimination of senescent cells in aged organisms could serve as a new strategy that may prevent or delay the process of aging and occurrence of comorbidities. Indeed, aging and senescence are not synonymous as senescent cells occur at any life stage, from embryogenesis to adulthood.[9] Cells found in tissues of aging animals tend to occur at different stages of cellular aging, including replicative aging and cellular senescence.[10] One common characteristic of senescent cells is an essentially irreversible cell-cycle arrest while remaining metabolically active. A further characteristic is the secretion of senescence-associated secretory phenotype (SASP) factors. Evidence suggests that the role of the SASP is to induce immune clearance.[11] However, senescent cells also negatively affect non-senescent cells through reactive oxygen species and the SASP in a paracrine manner, creating a harsh environment for them.[9,12] Another interesting report showed senescent cells communicate with neighboring cells by direct intercellular protein transfer.[13] Although numerous studies have investigated the adverse effects of physiological aging on salivary gland structure and functioning, the understanding of molecular mechanisms underlying the regulation of aging cells and the SASP of salivary glands remains incomplete.[14]

Therefore, we investigated three specific topics. First, the clinicopathological phenotypes of aged salivary glands were characterized, particularly focusing on the inflammatory microenvironment and its role during aging at the cellular and tissue levels such as the activation of the inflammatory response and the infiltration of immune cells. Second, we performed high-throughput RNA sequencing (RNA-seq) to explore the underlying mechanism at the molecular level and to infer key regulatory pathways. Global transcriptomic analyses revealed that genes associated with several metabolic pathways were enriched in the elderly, and we found evidence for a negative correlation between inflammatory factors and salivary gland functioning. Furthermore, we observed increased immune status in aged glands. Third, in combination with 18F-FDG PET/CT and histology, we used a rat model of natural aging to validate our clinical results. Improving our understanding of how aging regulates the inflammatory microenvironment and immune responses may inspire novel therapeutic avenues for disease treatment and/or prevention.

RESULTS

Clinicopathological characterization of young and aged minor salivary glands

Investigation of clinicopathology in salivary glands revealed glandular tissue-specific characteristics in young versus aged salivary glands. A flowchart of the study design is shown in Figure 1A. Varying degrees of atrophy were macroscopically observed in aged labial salivary glands (LSGs), and photos were taken to illustrate the significant size differences between young adult and aged LSGs (Figure 1A). Histological staining was performed using labial biopsy samples from younger adults (20–35 years old, female, n = 12) and older adults (≥65 years old, female, n = 12). We performed comprehensive histological analyses for regional differences with regard to the acini, myoepithelium, ducts (Figure 1B), blood vessels, and the extracellular matrix (ECM) surrounding acini and ducts (Figure 1C). Two types of acinus morphology were distinguished through H&E staining: serous acini, showing abundant basophilic cytoplasm with a round nucleus, and mucous acini with slightly basophilic cytoplasm. H&E staining indicated that the amount of acinar tissue decreased, and epithelium regions of larger excretory ducts varied in morphology from pseudostratified or stratified columnar to simple thin cuboidal in aged compared with younger LSGs (Figure 1D). Periodic acid-schiff (PAS) and Alcian blue special staining showed a large proportion of acini in salivary glands (Figure S1), which indicated these cells were producing neutral or acidic mucopolysaccharides. As expected, young salivary glands expressed abundant mucins and secretory activity, as shown through PAS and Alcian blue staining, while the acini cell population was strongly decreased in the aged (Figures 1D and 1E). Cytokeratin 7 (CK7) is a reliable marker of the ductal epithelium,[15] and VEGF (vascular endothelial growth factor) is a marker for angiogenesis and vascular permeability, which can be produced by endothelial cells, tissue cells, and inflammatory cells. A substantial reduction in acinar cells and ductal epithelium was observed accompanied by a decrease in VEGF expression in aged salivary

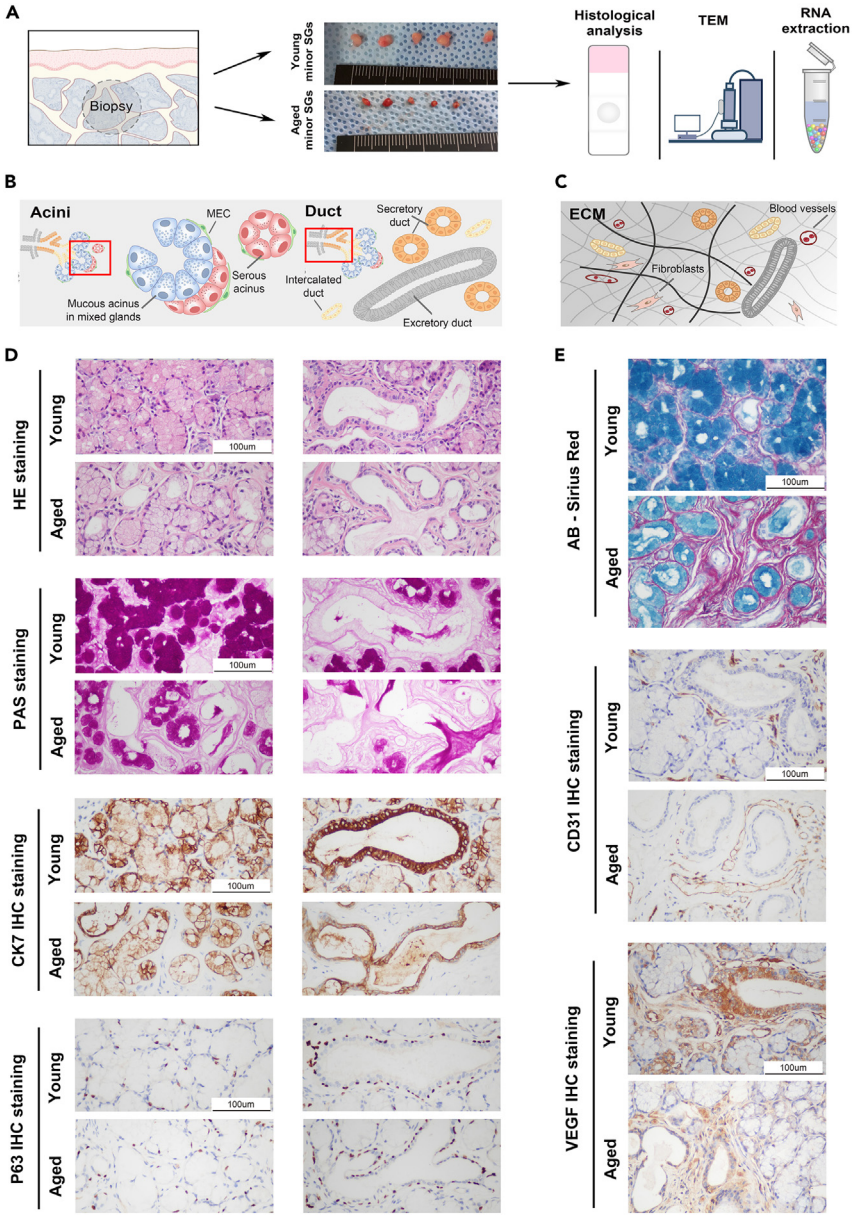

Figure 1. Clinicopathological characterization of young and aged minor salivary glands

(A) Illustration of the study design and representative clinical photos of young and aged labial salivary glands to assess the correlation between aging and glandular microenvironment by histology, TEM, and next-generation sequencing.

(B and C) Schematic diagrams showed distribution and structural features of (B) acini, ducts, and (C) interstitial tissue in minor salivary glands.

(D) Representative macroscopic pictures of hematoxylin and eosin (H&E) staining, Periodic acid-Schiff (PAS) staining, and immunohistochemistry (IHC) for Cytokeratin 7 (CK7), a marker for epithelial cell, and P63, a marker of myoepithelial cell in the acini and ducts of labial salivary glands. Scale bars: 100 μm, n = 12 per group.

(E) Representative macroscopic pictures of Alcian blue (AB)-Sirius red staining and IHC for CD31, a marker for microvessel density, and VEGF, a marker for angiogenesis in glandular interstitial tissue. Scale bars: 100 μm, n = 12 per group.

glands (Figures 1D and E and S1). Combined with the endothelial marker CD31, we observed abundant capillaries penetrating between acini or in the interstitial space. Fibrosis and collagen deposition are closely associated with aged morphological remodeling.[2] Through Sirius Red staining, collagen appears red in bright-field imaging, and it appears red or green-yellow in polarized light. Accordingly, Sirius Red staining (Figure 1E) delineated areas of collagen deposition, which was increased in the aged ECM

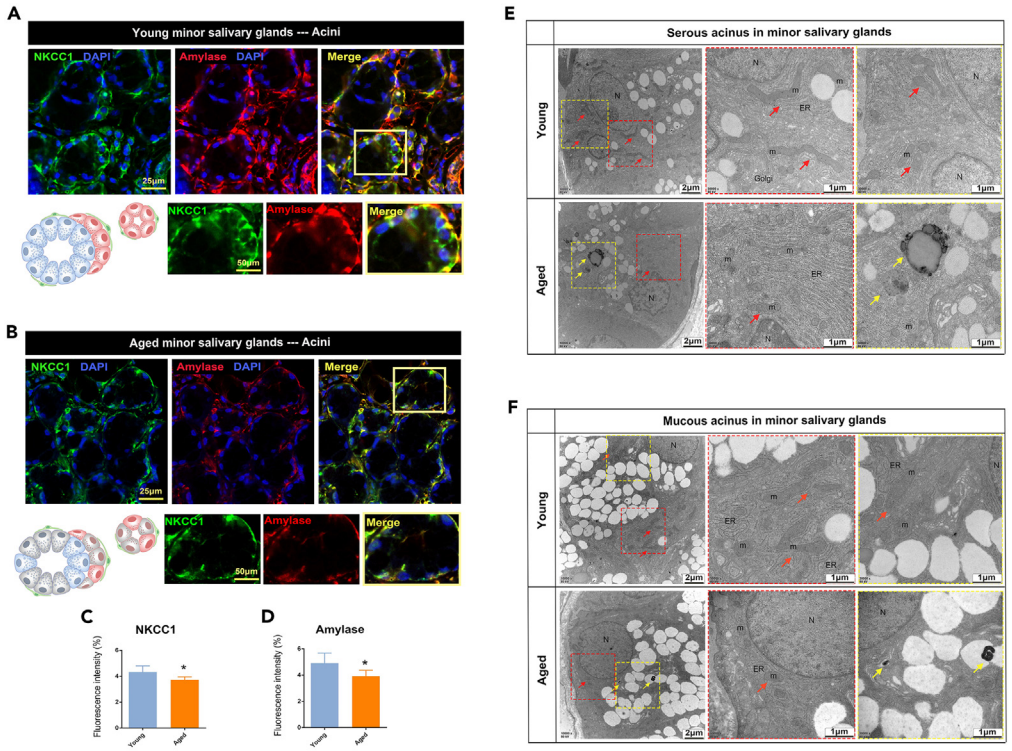

Figure 2. Age-related morphological and functional changes in minor salivary gland acini

(A and B) Co-localization by confocal microscopy of NKCC1 (green), Amylase (acinar cell marker) (red), and DAPI (blue) in (A) young and (B) aged minor salivary gland acini indicated at upper row. Enlargements from each of the panels were shown at lower row. Scale bars: 25 μm; 50 μm (magnified).

(C and D) Semi-quantitative evaluation of fluorescence intensity of (C) NKCC1 and (D) Amylase as in (A) and (B). Error bars indicate SD. *$p < 0.05$, $n = 8$ per group.

(E) Representative transmission electron microscopy (TEM) images of serous acinus in young and aged minor salivary glands. Red arrows indicated mitochondria (m). In contrast to the young ones, several autophagolysosomes (yellow arrows) were observed in the cytoplasm of the aged acinar cell ($n = 6$).

(F) Representative TEM images of mucous acinus in young and aged minor salivary glands. Red arrows indicated mitochondria (m), and yellow arrows (lower row) indicated the accumulation of lysosomes in the cytoplasm of the aged mucous acinar cell ($n = 6$).

compared to young ECM (Figure S1). Cells positive for basal marker P63 (a myoepithelial cell marker, nuclear staining) were also present and were consistently located in the outer layer of acini and ducts. We counted the number of P63-positive cells using a semi-quantitative method; there was no significant change in P63-positive cell numbers between young and aged LSGs (Figure S1).

Age-related morphological and functional changes in minor salivary glands acini and ducts

One of the most abundant proteins identified from saliva was salivary amylase, a glucose-polymer cleavage enzyme that is produced by the salivary glands. Under normal conditions, salivary glands mediate fluid secretion that requires basolateral Cl− influx via Na+-K + -2Cl− cotransporter isoform 1 (NKCC1), which imports Na+, K+, and 2Cl− into the cell across the plasma membrane.[16,17] Therefore, it was of interest to determine the pattern of expression of NKCC1 relative to amylase. This was tested by immunolocalization of NKCC1 and amylase in the glandular tissue. The images in Figures 2A and 2B show that acinar cells stained positive for amylase were mostly within NKCC1 regions. Immunohistochemistry (IHC) analysis demonstrated less NKCC1 and amylase staining in the aged group (Figures 2C and 2D), indicative of reduced NKCC1 activity and salivary gland secretory function. The morphological characteristics of acinar cells were further examined through transmission electron microscopy (TEM). Serous acinar cell showed the ability to synthesize, store, and secrete proteins as the cytoplasm appeared filled with abundant zymogen granules and ribosomes attached to the surface of the rough endoplasmic reticulum (ER) and Golgi complex (Figure 2E). The nucleus of young serous acinar cells was surrounded by numerous

mitochondria and rough ER, indicative of active metabolism. In contrast, aged serous acinar cells displayed signs of cellular senescence, where the cytoplasm showed accumulation of large autophagolysosomes. The cytoplasm appeared rich in mucous secretory granules and Golgi complexes (Figure 2F), which was associated with active carbohydrate synthesis in mucous acinar cells, compared to serous acinar cells. In aged mucous acinar cells, mitochondria were smaller and less abundant than in young ones, and a similar accumulation of lysosomes was observed, which was rarely seen in the young group, suggesting lysosomal dysfunction in aged LSGs.

Fluid-secreting acinar cells and NaCl-absorbing duct cells are two functional types of duct cells. Duct cells secrete little fluid; however, they exert other important biological functions, such as transporting water or electrolytes, providing energy, and participating in saliva metabolism.[17,18] More evidence was provided by TEM images. The thinning of the luminal layer and lumen expansion were clearly visible in aged intercalated ducts (Figure 3A). At high magnification, the intercalated ductal cell appeared to contain less cytoplasm, accompanied by a small number of Golgi complexes, rough ERs, and free ribosomes, which are some characteristics of serous acinar cells. Like other epithelial cells with apical-basal polarity, secretory and excretory ductal cells have an apical and a basal surface. Mitochondria docked at the basal surface were abundant in young secretory and excretory ductal cells, and the mitochondria exhibited well-formed cristae, depending on their functional state (Figures 3C and 3F). In contrast to young ductal cells, aged ductal cells showed fewer mitochondria and more autophagolysosomes. E-cadherin (ECAD) is an intercellular junction and global epithelial marker. ECAD is a single-span transmembrane protein that directly mediates intercellular adhesion, maintains epithelial integrity, and is involved in epithelial cell proliferation and differentiation.[19] To investigate whether aging impacts the distribution of these proteins, we applied immunofluorescence (IF) staining to LSG sections. In normal salivary glands, ECAD is localized in the cell membrane of acinar and ductal cells. Intercalated ductal cells exhibited a well-organized tubular structure with a single layer of epithelial cells (Figures 3B and 3G). Expression of CK7 and ECAD protein was detected in most intercalated, secretory, and excretory ductal cells, and almost all ductal cells exhibited positive immunostaining. Moreover, CK7 and ECAD were abundantly expressed in excretory ductal cells of young LSGs, whereas aged LSGs exhibited low levels of CK7 and ECAD immunoreactive signals (Figures 3D and 3E). Taken together, we conclude that acinar cells continuously produce saliva and secretory proteins. One of the characteristics of secretory and excretory ductal cells is that they contain large amounts of mitochondria, owing to the constantly high energy requirement for salivary gland secretion and metabolism. During aging, salivary gland morphology undergoes progressive changes, which are accompanied by a corresponding adaptation of function.

Dramatic metabolic reprogramming and impaired oxidative phosphorylation (OXPHOS) are associated with salivary glandular function during the glandular aging process

To understand the potential molecular mechanisms involved in gland-specific aging, we performed whole transcriptome analysis via RNA-seq and evaluated pathway activation via gene set enrichment analysis (GSEA) in young and aged LSGs. GSEA analysis showed that several pathways involved in glycolysis gluconeogenesis, galactose metabolism, Notch signaling pathway, arachidonic acid metabolism, glycerolipid metabolism, lysosome, metabolism of xenobiotics by cytochrome P450, fatty acid metabolism, and glutamate metabolism were enriched in aged LSGs (Figure 4A). Cells produce adenosine triphosphate (ATP) via glycolysis and OXPHOS, which is essential for sustaining cellular functions.[20] The top enriched pathway glycolysis glyconeogenesis, ranked in Kyoto Encyclopedia of Genes and Genomes (KEGG) pathways, was independently shown in Figure 4B. To gain further insights into the relationship between the mitochondrial respiratory chain and salivary gland functioning, we performed fluorescent double-staining to examine co-localization of COXIV/NKCC1 and COXIV/CK7. COXIV, the terminal enzyme complex of the mitochondrial electron transport chain, is one of the nuclear-encoded subunits of cytochrome *c* oxidase. It is located in mitochondrion inner membrane and is frequently used as a mitochondrial resident protein marker. COXIV+ cells were present in most of the ductal cells (Figures 4C and 4D), which suggested that mitochondria were abundant in these regions, consistent with the results of TEM. COXIV+ cell abundance was positively correlated with NKCC1 and CK7 in the same tissue. One aged duct with marked atrophy exhibited weak red fluorescence intensity (Figure 4C, bottom row, top left corner), whereas a different aged duct exhibited regionally decreased red fluorescence intensity although with normal morphology (lower right corner). Semi-quantitative measurements of fluorescence intensity showed gradually downregulated expressions of COXIV, NKCC1 (Figure 2C), and CK7 (Figure 3D) with age. This indicated a dynamic process of impairment of mitochondrial functioning, which is frequently accompanied by impairment of salivary gland functioning in the aged.

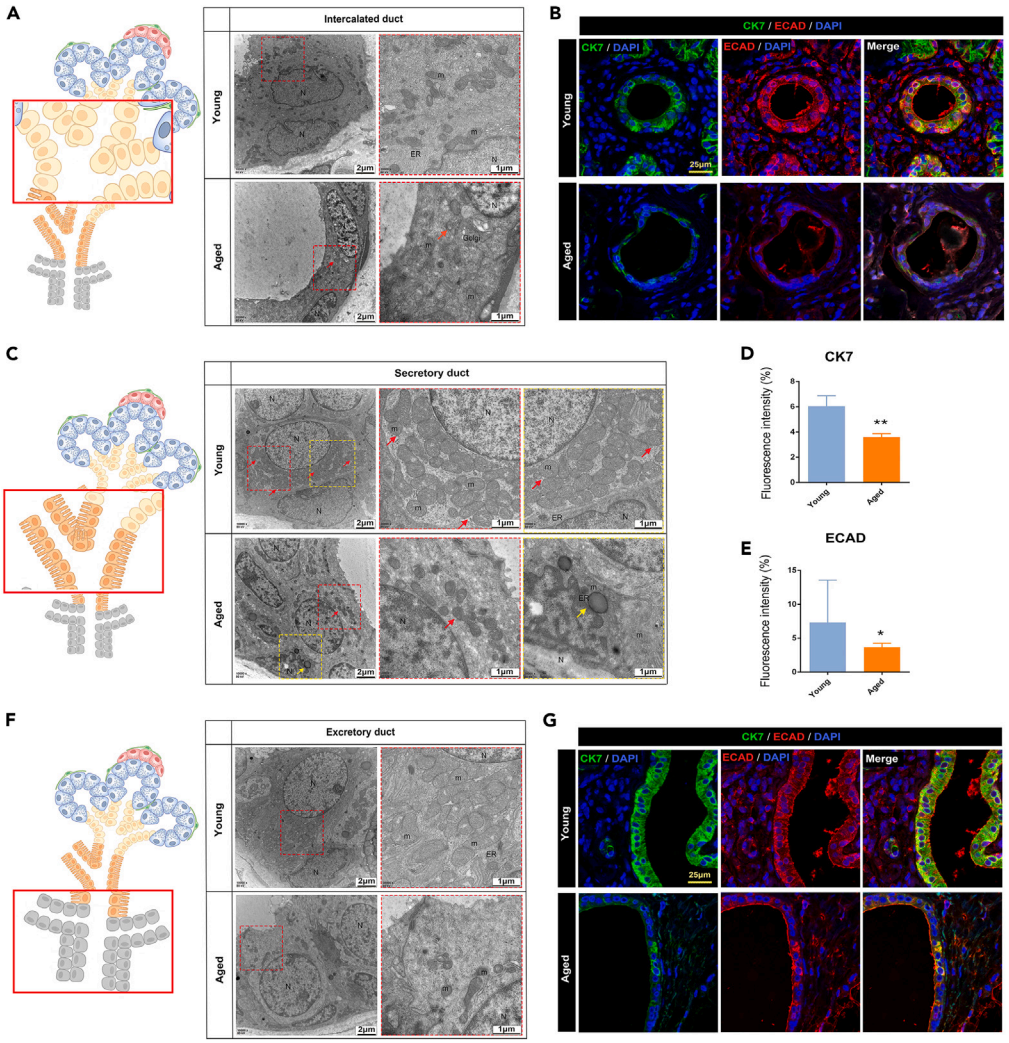

Figure 3. Age-related morphological and functional changes in minor salivary gland ducts

(A) Representative TEM images of intercalated duct in young and aged minor salivary glands. Red arrows indicated mitochondria (m) (n = 6).

(B) Co-localization by confocal microscopy of CK7 (green), E-cadherin (ECAD, the epithelial cell-cell adhesion protein as a lateral/basal marker) (red), and DAPI (blue) in young and aged minor salivary gland intercalated duct. Scale bars: 25 μm, n = 8 per group.

(C) Representative TEM images of secretory duct in young and aged minor salivary glands. Red arrows indicated mitochondria (m), and yellow arrow (lower row) indicated an autophagolysosome containing lipid droplets around the nucleus of aged ductal cell (n = 6).

(D and E) Semi-quantitative evaluation of fluorescence intensity of (D) CK7 and (E) ECAD as in (B) and (G). Error bars indicate standard deviation (SD). *$p < 0.05$, **$p < 0.01$, n = 8 per group; (F) Representative TEM images of excretory duct in young and aged minor salivary glands. Mitochondria (m, upper row) were extremely abundant in young, while in aged region (lower row), mitochondria were either absent or degenerated (n = 6); (G) Co-localization by confocal microscopy of CK7 (green), ECAD (red), and DAPI (blue) in young and aged minor salivary glands excretory duct. Scale bars: 25 μm, n = 8 per group.

SASP factors link pro-inflammatory processes with cell cycle and DNA replication and metabolism in salivary glands

Salivary glands contain a heterogeneous population of cells, including serous acini (LPO (lactoperoxidase), AMY2B (amylase 2B), ANO1(anoctamin 1), and BHLHA15 (basic helix-loop-helix family, member a15)), mucous acini (AQP5 (aquaporin 5), NKX3-1 (NK3 homeobox **1**), and MUC5B (mucin 5B)), ductal epithelial (KRT7 (keratin) and KLK1 (kallikrein 1)), myoepithelial, and fibroblasts (COL1A1, FAP (fibroblast activation protein), LUM (lumican), and DCN (decorin)).[21–27] To assess whether OXPHOS was associated with a

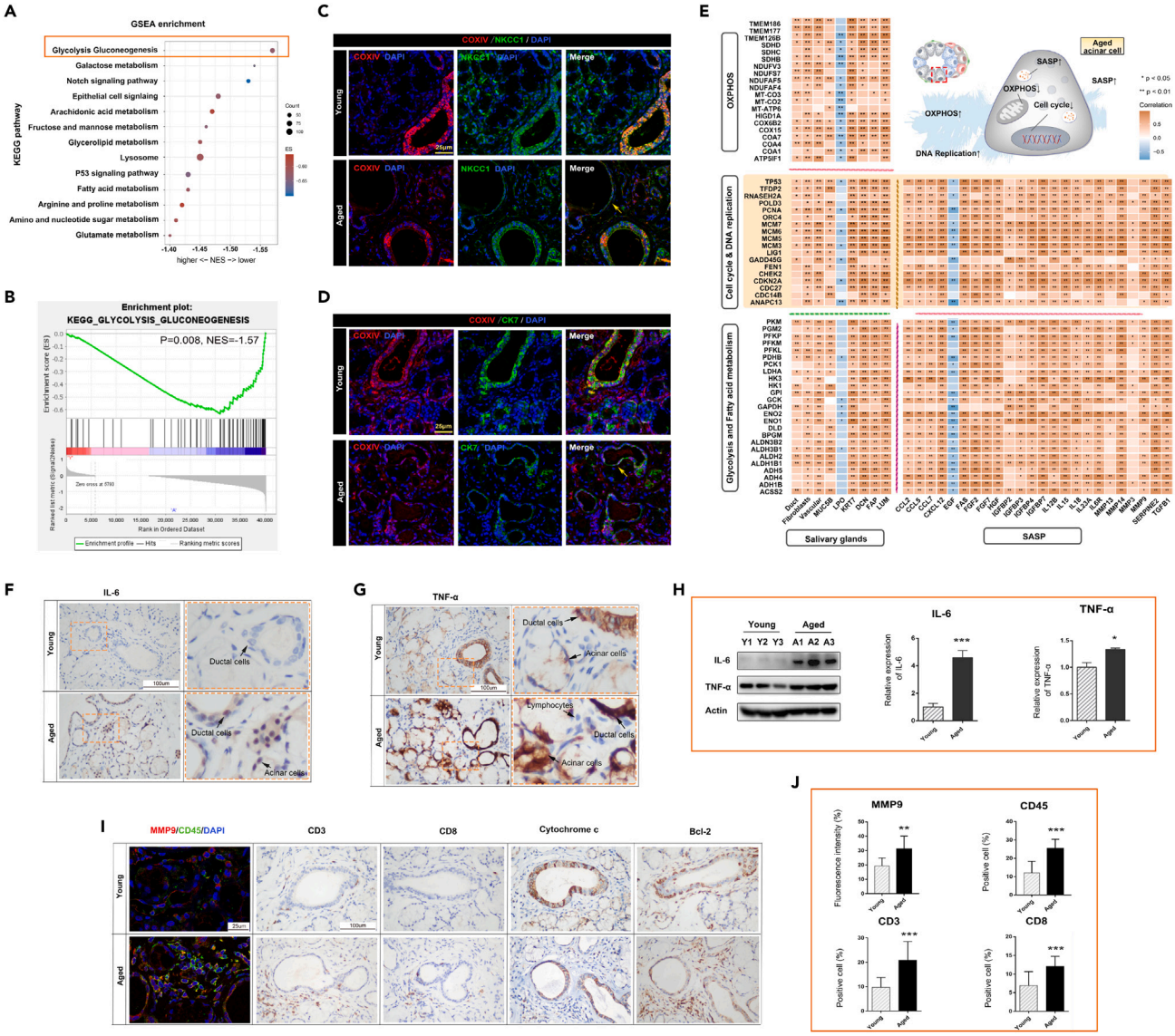

Figure 4. Metabolic reprogramming from oxidative phosphorylation (OXPHOS) to glycolysis had been found during glandular aging, which was associated with senescence-associated secretory phenotype (SASP) and immune response

(A) The bubble chart of the results of gene set enrichment analysis (GSEA) was generated using R package 'ggplot2'. The top 13 enriched KEGG pathways in response to phenotype aged of RNA-seq data were listed, in the order of normalized enriched score (NES).

(B) The top ranked gene set in the standard GSEA analysis was glycolysis glyconeogenesis gene set. Enrichment score was shown on the y axis as the relevant genomic features traversed on the x axis. FDR, false discovery rate.

(C) Co-localization by confocal microscopy of mitochondrial protein COXIV (green), NKCC1 (red), and DAPI (blue) in young and aged minor salivary glands. Scale bars: 25 μm, n = 8 per group.

(D) Co-localization by confocal microscopy of COXIV (green), CK7 (red), and DAPI (blue) in young and aged minor salivary glands. Scale bars: 25 μm, n = 8 per group.

(E) Correlation of OXPHOS genes, cell cycling & DNA replication genes, glycolysis and fatty acid metabolism genes with SASP factors and salivary gland function genes. Correlation statistics and the related p value were computed using Spearman correlation. *$p < 0.05$, **$p < 0.01$.

(F) IHC staining for IL-6. Scale bars: 100 μm, n = 12 per group.

(G) IHC staining for TNF-α. Scale bars: 100 μm, n = 12 per group.

(H) Western blot for IL-6 and TNF-α between young and aged groups. Bar graph showed semi-quantitative analysis of western blot about IL-6 and TNF-α protein expression. Relative protein expression is represented as the optical density ratio of targeted protein to actin. Data are expressed as the mean ± SD. ***$p < 0.001$, vs. young group (n = 3). All experiments had been repeated at least twice, with similar results.

(I) MMP9/CD45 co-localization was visualized by immunofluorescence (IF) staining and IHC for CD3, CD8, cytochrome c, and Bcl-2. Scale bars: 25 μm (IF); 100 μm (IHC), n = 12 per group; (J) Semi-quantitative IF or IHC analysis for showing percentage of MMP9, CD45, CD3, and CD8 positive cells using ImageJ in young and aged labial salivary glands. Error bars indicate SD. *$p < 0.05$, **$p < 0.01$, ***$p < 0.01$, n = 12.

pro-inflammatory microenvironment and salivary gland functioning, the correlation between OXPHOS genes and hub genes (SASP factors and salivary gland-specific genes) was calculated using Spearman's rank correlation and was visualized using the R package 'ggplot2' based on RNA-seq data. The results showed OXPHOS marker genes were positively correlated with cell cycle and DNA replication genes and salivary gland functional genes (Figure 4E) but negatively correlated with SASP factors in the whole glandular microenvironment (Figure S2). Of note, SASP factors were positively correlated with cell cycle & DNA replication genes and glycolysis and fatty acid metabolism genes. To characterize the inflammatory microenvironment and immune response in aged salivary glands, histological staining and microscopic analysis were performed. Immunohistochemistry staining showed that interleukin-6 (IL-6) was rarely expressed in the young LSGs, while their expression was remarkably elevated in ductal cells and acinar cells of aged LSGs (Figure 4F). We observed ductal cells and acinar cells of aged LSGs that produced abundant levels of tumor necrosis factor alpha (TNF-α) and lymphocytes that expressed little TNF-α (Figure 4G). Similarly, results of Western blot (WB) analysis showed that the expression of IL-6 and TNF-α was significantly upregulated in aged LSGs compared to that in the young LSGs (Figure 4H).

Based on previous reports in the literature, plasma cells, B lymphocytes, T cell subtypes ($CD8^+$ T and Tfh), and myeloid-derived cells represent dominant immune cell populations in salivary glands.[21] Matrix metalloproteinase 9 (MMP9) has a major role in regulating tissue remodeling by degrading ECM and activation of leukocyte behavior. Senescent cells can develop SASP, such as matrix metalloproteinases and pro-inflammatory cytokines, and this pro-inflammatory secretome may contribute to senescence.[1,28] Here, fluorescent-labeled antibodies specific for MMP9 and CD45 were used to identify the SASP factor and myeloid-derived cells, respectively. MMP9/CD45-positive cells were found in aged LSGs, while few have co-localization of MMP9 and CD45 fluorescence in young LSGs (Figure 4I). We performed a semi-quantitative analysis of immunofluorescence images and noticed that pro-inflammatory factors show a significant increase in aged LSGs (Figure 4J). Histological staining revealed there was a scattered distribution of CD3- and CD8-positive cells in young LSGs and more lymphocytic infiltration in the periductal and interstitial areas dominated by $CD3^+$ and $CD8^+$ T lymphocytes in aged LSGs (Figure 4I). In intact viable cells, cytochrome *c* localizes to the mitochondrial matrix and plays an essential role in respiratory chain function, cellular energy consumption, and apoptosis.[29] When cells apoptosis occurs, Bcl-2 as an anti-apoptotic family protein prevents the release of cytochrome *c* from mitochondria.[30,31] IHC staining showed cytochrome *c* was mainly expressed in young ductal epithelial cells, detecting in mitochondria-rich regions of these cells. What is interesting is that significant Bcl-2 expression could be detected in myoepithelial cells and not in glandular epithelial cells. In aged LSGs, we found cytoplasmic cytochrome *c* expression was significantly decreased in glandular epithelium and scattered in connective tissue areas, whereas the expression of Bcl-2 was significantly increased. Taken together, these results revealed that salivary gland cellular senescence contributes to aging and decline in mitochondrial function; meanwhile, these aging cells might modulate their own cellular behavior, develop a persistent pro-inflammatory phenotype, and further impair cellular function.

Increased inflammation in the minor salivary glands with age coincides with increased immune response and altered metabolism

We hypothesized that aging-associated salivary gland dysfunction was due to accumulation of inflammatory factors in the gland microenvironment. To investigate this hypothesis, we first examined mRNA levels of pro-inflammatory factors IL-6 and TNF-α. qPCR analysis showed that IL-6 and TNF-α expression was significantly increased in aged LSGs compared to young LSGs (Figure 5A). We then assessed the distribution of p16INK4a and P53 in aged LSGs. The senescence program frequently occurred with upregulation of cell-cycle arrest and senescence markers.[10] Accumulation of P16INK4a and P53 proteins is associated with cell-intrinsic changes and molecular aging, and it is considered as senescence markers.[32] IHC for p16INK4a was largely negative in young LSGs, with a few acini and duct regions showing scattered P53-positive staining cells (Figure 5B). As expected, increased expression of p16INK4a protein was detected in ductal epithelium, whereas P53 expression was widely distributed in aged LSGs. Ultrastructure information on the inflammatory microenvironment in aged salivary glands is limited. TEM images showed different cell types in young and aged LSGs. As shown in Figure 5C, non-activated fibroblasts were predominant in connective tissue of young LSGs. In addition to the presence of fibroblasts (Figure 5D), connective tissue of aged LSGs was characterized by infiltration with inflammatory cells, including lymphocytes, plasma cells (Figure 5E), and mast cells (Figure 5F). To further investigate the potential relevance between the SASP and salivary gland microenvironment, including salivary gland-specific components, immune cells, and metabolism, log rank (Mantel-Cox) tests were used to assess the significance between two groups based on RNA-seq

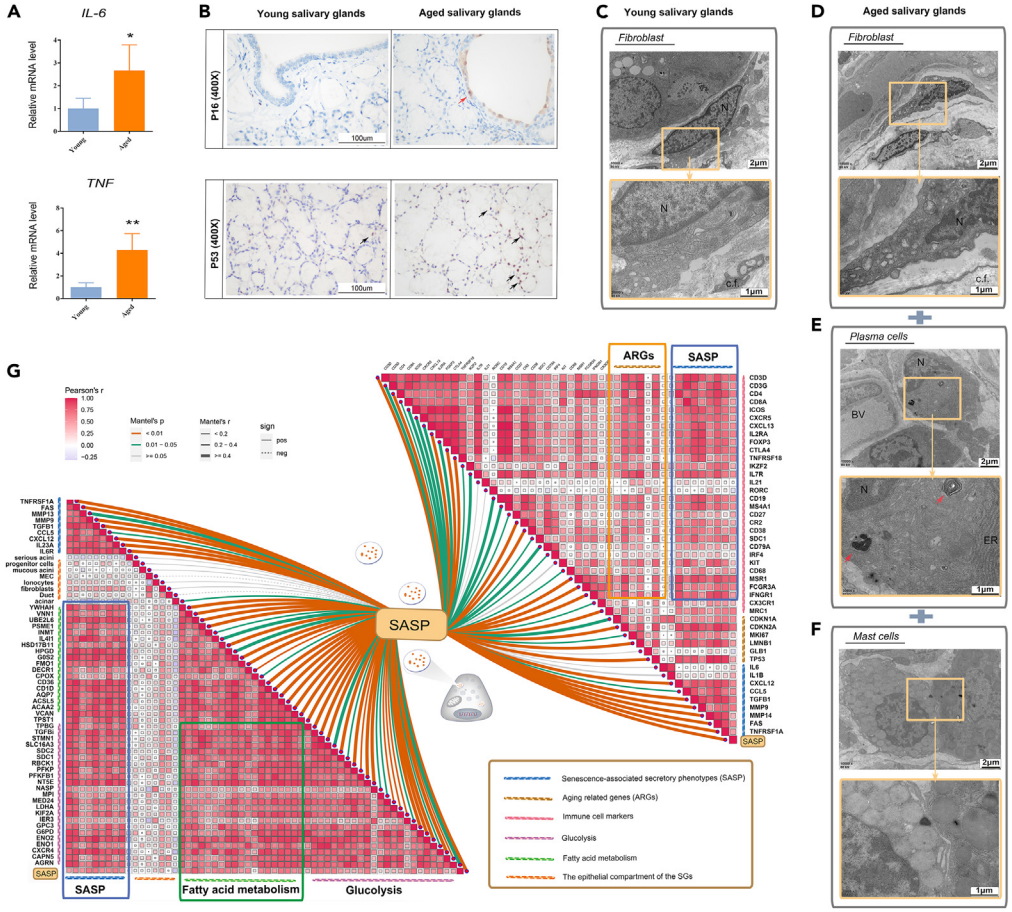

Figure 5. Increased inflammation in the minor salivary glands with age coincided with increased immune response and impaired metabolism

(A) Quantitative reverse transcription-PCR (qRT-PCR) analysis for pro-inflammatory factor gene expression (*IL-6* and *TNF-α*) (n = 3, bars and error bars represent the mean ± SD, *p < 0.05, **p < 0.01 by Student's *t* test relative to young subjects).

(B) Representative macroscopic pictures of IHC for senescence marker proteins, P16 and P53, in young and aged glandular tissue. Scale bars, 100 μm, n = 12 per group.

(C) Representative TEM images of fibroblasts in young glandular interstitial tissue, n = 6.

(D–F) Representative TEM images of (D) fibroblasts, (E) plasma cells, and (F) mast cells in aged glandular interstitial tissue, n = 6.

(G) Correlation between SASP and salivary gland microenvironment, including salivary gland-specific components, immune cells, and metabolism. Color bar represents the cross-correlation values (Pearson's correlation coefficients), with red color indicating positive correlation (Pearson's r > 0) and purple color indicating negative correlation (Pearson's r < 0). The statistical p value was generated by Log rank Mantel-Cox test, with orange line indicating p value < 0.01.

data. The results were visualized using the R package 'ggcor'. SASP genes were positively related to immune response and aging-related genes (ARGs) but negatively related to salivary acini functioning (Mantel's p < 0.05, Pearson's correlation) (Figure 5G). Furthermore, SASP genes were strongly correlated with genes involved in the senescence glycolysis and fatty acid metabolism. The above results show that aging epithelial cells of salivary glands deteriorated their microenvironment through the auto- and paracrine effects of the SASP, which thus may lead to a systemic alteration of numerous metabolic pathways.

Elevated levels of inflammatory phenotypes, impairment of mitochondrial activity, and reduced glandular function in natural aging rat model

To further verify inflammatory phenotypes in aging process, a natural aging animal model was established by raising Sprague-Dawley (SD) rats until they were 27 months old. qRT-PCR revealed that mRNA levels of pro-inflammatory factors IL-1β and IL-6 were significantly higher in salivary glands of aged rats than in young rats (p < 0.001, p < 0.05, respectively) (Figure 6A). The representative pictures

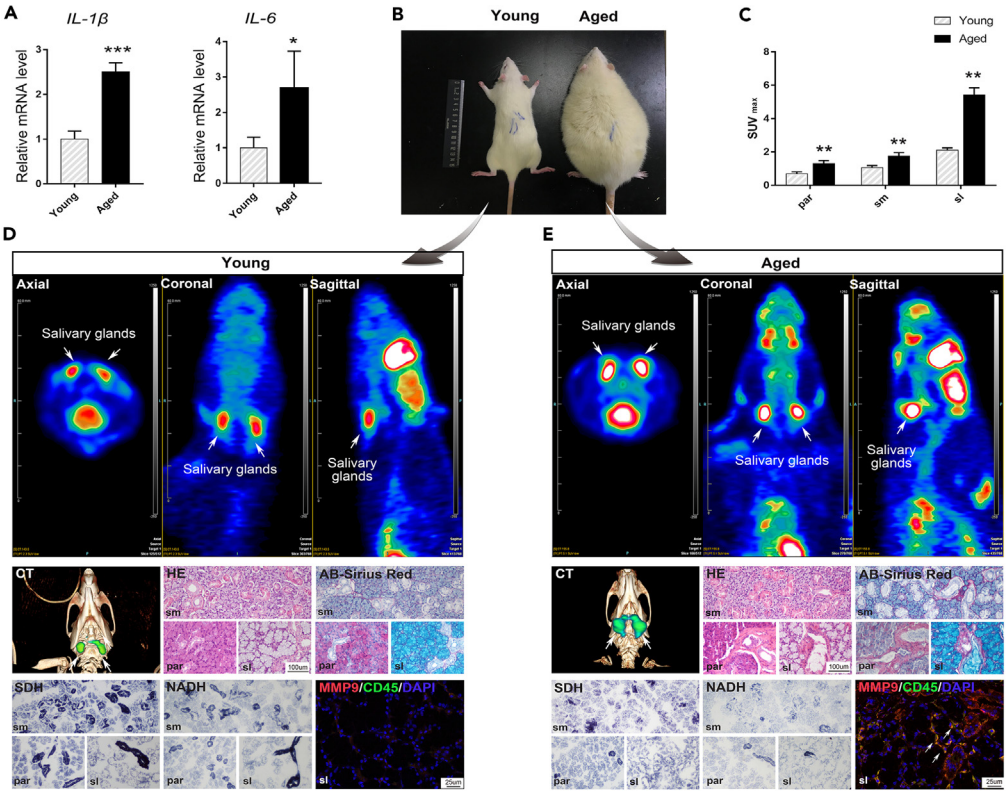

Figure 6. Elevated levels of inflammatory phenotypes, aggregation of immune cells, and reduced glandular function in the aged rat salivary glands

(A) qRT-PCR analysis for pro-inflammatory factor gene expression (*IL-1β* and *IL-6*) (n = 3, bars and error bars represent the mean ± SD, *p < 0.05; **p < 0.01 by Student's *t* test relative to young rats).

(B) A photograph of young (3-month-old) and aged (27-month-old) female rat.

(C) Standardized uptake values (SUVs) in salivary gland regions obtained from PET/CT images taken at young and aged groups. The absorption value of maximum SUV (SUV max) measured by FDG-PET was significantly higher in the aged group than the young group (n = 3, bars and error bars represent the mean ± SD, *p < 0.05; **p < 0.01). par parotid glands, sm submandibular glands, sl sublingual glands.

(D and E) Representative images of ^{18}F-FDG uptake by micro-PET/CT imaging, H&E staining, AB-Sirius red staining, succinic dehydrogenase (SDH)-specific staining, NADH-tetrazolium reductase (NADH-TR) staining, and co-immunofluorescent staining of MMP9 (green) and CD45 (red) in (D) young and (E) aged group. White arrow indicated gland tissue glucose uptake (n = 3).

of young and aged rats were shown in Figure 6B. Clinical 18F-FDG PET/CT is a widely noninvasive, highly sensitive imaging modality suitable for detection and follow-up of tumors, infections, and sterile inflammation. It is known that 18F-FDG uptake is upregulated in inflammatory lesions with pro-inflammatory myeloid cells such as neutrophils and macrophages.[33,34] Here, positron emission tomography with 2-deoxy-2-18F-fluoro-D-glucose integrated with CT (18F-FDG PET/CT) was used to assess the inflammation condition in aged rat salivary glands. Three major salivary glands, including parotid glands (par), submandibular glands (sm), sublingual glands (sl) were delineated on multiple coronal PET slices with the help of matched CT images. The standardized uptake values (SUVs) of par, sm, and sl were 1.3 ± 0.18, 1.75 ± 0.21, and 5.43 ± 0.43, respectively, in the aged group, higher than those of the young group (0.69 ± 0.11, 1.01 ± 0.12, and 2.1 ± 0.14, $p < 0.01$) according to the semi-quantitative analysis (Figures 6C–6E). The results indicated that aged salivary glands show an increased inflammatory signaling compared to that in the young rats. It was further verified by co-immunofluorescent staining, which documented the increased distribution of MMP9+/CD45+ cells in aged rat sublingual glands (Figures 6D and 6E), consistent with a previous report.[35] We next evaluated whether aging would impact salivary gland function using our natural aging animal model. H&E and AB-Sirius red staining showed acini atrophy, ducts expanded, and collagen deposition in aged rats (Figures 6D and 6E); this phenotype

is similar in humans as well. Otherwise, succinic dehydrogenase (SDH) and NADH staining were used to visualize the activity and distribution of the mitochondrial respiratory chain. SDH and NADH enzyme activities were clearly detected in salivary glands of young rats, while they were greatly reduced in aged rats, with statistically significant differences (Figure S3).

DISCUSSION

Salivary gland aging is a multistage, multifactorial process, frequently leading to impaired functioning of the glands.[36] In the current study, coordinated analyses of various data from histology, ultrastructure information, gene expression, transcriptomics, and aged animal models produced integrated insights into aging phenotypes of salivary glands at multiple levels.

Morphological observations in the present study revealed that phenotypic differences become evident with age. First, there was a gradual change in the mean volume of acini, as well as a gradual increase in fibrotic and adipose tissue in salivary glands, which is in line with the results of previous studies.[2,36] Moreover, aged LSGs exhibited weak cytoplasmic AB and PAS staining, suggesting a decreased functioning with regard to mucin secretion. The increase in adipose and fibrous connective tissue was previously reported to contribute to aging-associated degeneration and decline of glandular function.[36] Using TEM, we discovered, for the first time, the occurrence of mast cells in the connective tissue matrix of aged human salivary glands. The important role of the innate immune system in various fibrotic diseases has become apparent recently. Mast cells have been considered to be among the most important participants in inflammatory processes involving fibrosis owing to their secretion of tryptases involved in connective tissue breakdown.[37] Moreover, the acinar lumen is the initial site of saliva secretion. Cl−-reuptake is an important saliva secretion mechanism, and approximately 70% of this reuptake is accomplished by the NKCC1 cotransporter.[38] In the current study, we found that NKCC1/amylase fluorescence intensity was decreased within aged acini and ducts, compared to those of young subjects, indicating that Cl−-reuptake and saliva secretion are impaired in aged glands. This helps explain why saliva production is decreased during aging, which leads to xerostomia. Notably, high columnar cells within young excretory ducts showed the strongest reaction for CK7 and ECAD, whereas only residual expression of CK7 and ECAD occurred in aged ducts. ECAD is essential for the maintenance of cell-cell adhesion and regulation of tissue homeostasis by modulating various signaling pathways. Functional loss of ECAD in epithelial cells is considered a hallmark of epithelial-mesenchymal transition (EMT).[19] EMT-dependent fibrosis appears to be associated with autoimmune conditions and unresolved inflammatory response. Multiple pro-inflammatory signals (such as transforming growth factor β [TGF-β]), affecting the EMT program in a switch-like manner, activate a pathological fibrotic state, which was recently found to be associated with salivary gland atrophy and fibrosis.[39,40] Thus, compounds interfering with EMT or EMT-associated transcription factors are considered promising anti-fibrotic drug targets in various organ fibrosis animal models; however, this remains to be examined in clinical trials.[39,41]

Recent studies established that aging not only results in cell-autonomous alterations but also causes changes at the level of intercellular communication, referred to as ''inflammaging''.[1] Inflammaging can impair cellular functions in nearby cells, modulate the aging cells' microenvironment, and reinforce its interaction with the immune system by developing a persistent pro-inflammatory phenotype.[42] Hallmarks of cell-autonomous alterations include irreversible growth arrest, mitochondrial dysfunction, SASP production, and apoptosis resistance.[43] In current study, several lines of evidence demonstrated the multiple phenotypes of aging cells in salivary glands. On the molecular level, we analyzed our RNA-seq datasets for genes, and GSEA analyses revealed OXPHOS pathway genes were closely related to the whole glandular microenvironment. OXPHOS, consisting of the respiratory chain and the ATP synthase complex, is the core mitochondrial pathway responsible for ATP synthesis.[44] Age-associated mitochondrial dysfunction represents an intrinsic driver of aging.[1,45] When cells and organisms age, the efficacy of OXPHOS tends to decrease, resulting in reduced ATP synthesis. Furthermore, mitochondria are key contributors to the development of the senescent phenotype, particularly the SASP,[9,46] which was also confirmed by bioinformatics analyses. We then assessed mitochondrial protein COXIV localization in acinar and ductal cells. IF staining indicated a substantially decreased overlap of COXIV with NKCC1 and CK7 in aged glandular cells, suggesting that mitochondrial functioning is critical for the maintenance of salivary gland function.

In-depth understanding of cellular architecture is essential for understanding glandular biology and functioning. On the cellular level, we present detailed electron microscopy images of whole tissues with respect

to young and aged LSGs. It's interesting that mitochondria were abundant in secretory and excretory ductal cells in young LSGs, indicating active energy supply for transcellular transport in this region. Furthermore, in aged LSGs, acinar and ductal cells displayed typical characteristics of aging cells, such as signs of accumulation of lysosomes and autophagolysosomes, and mitochondrial damage. Increasing evidence suggests a negative correlation between autophagy and aging.[47] The presence of undigested materials in lysosomes may be responsible for their impaired ability to degrade intracellular components (autophagy).[47,48] Mitochondrial dysfunction temporally occurs earlier than lysosomal dysfunction, and the interplay between mitochondria and lysosomes in aging cells is a further topic of interest. A gradual decrease of mitochondrial and autophagic activity with age may play an important role in the functional decline of gland function in the aging human salivary gland. Additional studies are necessary to understand the underlying mechanisms to determine whether a combination therapy targeting mitochondrial dysfunction and insufficient autophagy are effective against aging-associated pathologies.[45]

Although senescent cells may transiently exert beneficial effects, their chronic accumulation in various tissues and organs during aging has detrimental consequences.[43,49] In addition, the cellular microenvironment has also become an area of intense research. The SASP may be a double-edged sword as it can deteriorate the microenvironment and impair cellular functions in nearby cells; however, it can recruit immune cells and activate an immune surveillance response to clear senescent cells.[49] In the present study, we identified multiple SASP factors controlling salivary gland aging, including VEGF, TNF-α, IL-1β, and IL-6. The multiple components of the SASP can amplify the response and execute paracrine senescence.[50] Previous studies have reported that mTOR (mechanistic target of rapamycin) inhibitor rapamycin, as a potent SASP suppressor, helps maintain tissue homeostasis by alleviating chronic low-level inflammation in aged tissues.[51] However, the inhibition of mTOR can also impair immune surveillance and accelerate accumulation of senescent cells and aging. Further research is required to develop potent selective SASP inhibitors for clinical applications. We found that SASP factors in minor salivary glands coincided with a systemic alteration of numerous metabolic pathways during aging, including glycolysis and fatty acid metabolism. We report increased 18F-FDG uptake in major salivary glands of aged rats. FDG uptake occurs in cells exhibiting increased glycolysis and in inflammatory lesions. As senescent cells exhibited mitochondrial dysfunction according to TEM results, we speculate that decreased mitochondrial function in aged salivary glands results in a decline in energy production, which may cause metabolic reprogramming toward additional energy production. This may explain their dependence on glycolysis for ATP production.[46]

Aging is a complex process characterized by a progressive loss of physiological functions in multiple tissues and systems. Whether or how this process controls salivary gland immune responses remains unknown. In the current study, using immunohistochemical immune markers, increased immune cell infiltration ($CD3^+$ T cells, $CD8^+$ T cells, and myeloid cells) in the connective tissue of aged LSGs was observed. This suggests that senescent cells can recruit immune cells to facilitate their own elimination. We thus propose that immune cells were driven by the inflammatory signals initiated by SASP factors generated by senescent cells. One of the functions of the immune system is involved in the recognition and elimination of senescent cells.[1] Immune cells, such as natural killer (NK) cells, macrophages, and T cells, can eliminate senescent cells in virous tissues.[42] However, the immune system undergoes profound transformations during natural aging. In the current study, glandular respiratory chain impairment in aged rats was accompanied by an increased inflammatory microenvironment. This finding is surprising given the well-established association of changes in immune function due to aging termed "immunosenescence". Such immunosenescence displays chronic inflammation and gradual deterioration of adaptive immune function, thus causing elevated accumulation of senescent cells with age.[52–54] Various aspects of the innate and adaptive immune systems appear to be affected by aging; however, the adaptive immune system, in particular, T lymphocytes, are likely affected the most.[53,55] The effect of aging on immune cells is more complex than previously appreciated. A recent study using a lymphoid organ-specific Ercc1-knockout model[52] showed that aged immune cells failed to suppress senescence. The regulation of senescent cells by the immune system opens a new area of research. An aged senescent immune system would promote systemic aging and inflammation and disrupt tissue homeostasis that contributes to reduced lifespan and therefore also represents a key therapeutic target to extend healthy aging.[42]

In summary, we found distinct changes in the salivary glands that characterize aging are accompanied by acini atrophy, ducts expanded, collagen deposition, reduced mitochondrial respiratory chain activity,

and inflammatory microenvironment, which might reflect progressive degeneration of salivary gland function. Our study revealed several aspects of complex cellular cross-talk among aging acinar cells, inflammatory factors, and the immune response. The significance of these findings is that they provide further mechanistic insights into age-related clinicopathogenesis, important implications for early diagnosis, increased choice of therapy, and identification of new targets for improving salivary gland dysfunction.

Limitations of the study

Salivary glands contain a heterogeneous population of cells, including glandular epithelial cells, myoepithelial cells, fibroblasts, and vascular cells, as well as immune cells. What's more, there are numerous cell subsets within each immune cell (T cell, B cell, NK cell, dendritic cell (DC), macrophage, and other lineages), and aging cells are also divided into different stages. Analysis of pooled cell populations by RNA-seq does not enable the identification of the cell types that express certain genes but instead provides a virtual average of the multiple cellular components. As single-cell RNA-seq (scRNA-seq) enables rapid determination of the precise gene expression patterns of thousands of individual cells, we anticipate that future work will utilize scRNA-seq to investigate gland tissue cell heterogeneity. Second, there are several possible senescence-targeted therapeutic approaches, including senescent cell removal and SASP inhibition.[56] Although our results are successfully validated in a naturally aged rat model, the effectiveness of senescence-targeted therapies has yet to be assessed. Further research and validation studies are needed. In addition, pathology in the minor salivary glands may not completely reflect pathology found in the major salivary glands. Alternatively, there may be microenvironmental differences between the parotid and LSG tissues, although researchers observed a strong correlation between average gene expression in PSGs and LSGs.[57] Future studies comparing aged minor salivary glands to the aged major salivary glands are warranted. In the follow-up work, we will continue to study the molecular mechanism in salivary gland aging.

STAR★METHODS

Detailed methods are provided in the online version of this paper and include the following:

- KEY RESOURCES TABLE
- RESOURCE AVAILABILITY
  - Lead contact
  - Materials availability
  - Data and code availability
- EXPERIMENTAL MODEL AND SUBJECT DETAILS
  - Patients and specimens
  - Natural aging rat model
- METHOD DETAILS
  - Histological analysis
  - Transmission electron microscopy (TEM)
  - Western blot
  - RNA extraction and quantitative reverse transcription-PCR (qRT-PCR)
  - RNA sequencing (RNA-seq) data and gene expression analysis
  - Bioinformatic evaluation and analysis
  - Animal procedures
  - Micro-PET/CT scan and image reconstruction
- QUANTIFICATION AND STATISTICAL ANALYSIS

SUPPLEMENTAL INFORMATION

Supplemental information can be found online at https://doi.org/10.1016/j.isci.2023.106571.

ACKNOWLEDGMENTS

This work was assisted by Core Facility of Basic Medical Sciences, Shanghai Jiao Tong University School of Medicine.

AUTHOR CONTRIBUTIONS

N.L.: Conceptualization, Methodology, Formal analysis, Writing - Original Draft. Y.Y.: Validation, Investigation, Writing - Original Draft. Y.W.: Validation, Investigation, Visualization. J.H.: Software, Investigation, Visualization. L.L.: Investigation, Resources. D.L.: Software, Data Curation. Y.L.: Investigation. J.Y.: Investigation. Y. G.: Investigation. W.H.: Software, Writing - Review & Editing. Y.X.: Investigation, Writing - Review & Editing. L.J.: Conceptualization, Methodology, Supervision, Writing - Review & Editing, Project administration, Funding acquisition.

DECLARATION OF INTERESTS

The authors declare no competing interests.

Received: September 24, 2022
Revised: December 29, 2022
Accepted: March 28, 2023
Published: April 5, 2023

REFERENCES

1. López-Otín, C., Blasco, M.A., Partridge, L., Serrano, M., and Kroemer, G. (2013). The hallmarks of aging. Cell *153*, 1194–1217. https://doi.org/10.1016/j.cell.2013.05.039.

2. Toan, N.K., and Ahn, S.G. (2021). Aging-related metabolic dysfunction in the salivary gland: a review of the literature. Int. J. Mol. Sci. *22*, 5835. https://doi.org/10.3390/ijms22115835.

3. Smith, C.H., Boland, B., Daureeawoo, Y., Donaldson, E., Small, K., and Tuomainen, J. (2013). Effect of aging on stimulated salivary flow in adults. J. Am. Geriatr. Soc. *61*, 805–808. https://doi.org/10.1111/jgs.12219.

4. Pringle, S., Van Os, R., and Coppes, R.P. (2013). Concise review: adult salivary gland stem cells and a potential therapy for xerostomia. Stem Cell. *31*, 613–619. https://doi.org/10.1002/stem.1327.

5. Takamatsu, K., Tanaka, J., Katada, R., Azuma, K., Takakura, I., Aota, K., Kamatani, T., Shirota, T., Inoue, S., and Mishima, K. (2021). Aging-associated stem/progenitor cell dysfunction in the salivary glands of mice. Exp. Cell Res. *409*, 112889. https://doi.org/10.1016/j.yexcr.2021.112889.

6. Zhang, X., Zhou, J., Wang, X., Geng, J., Chen, Y., and Sun, Y. (2022). IFT140(+)/K14(+) cells function as stem/progenitor cells in salivary glands. Int. J. Oral Sci. *14*, 49. https://doi.org/10.1038/s41368-022-00200-5.

7. Aure, M.H., Arany, S., and Ovitt, C.E. (2015). Salivary glands: stem cells, self-duplication, or both? J. Dent. Res. *94*, 1502–1507. https://doi.org/10.1177/0022034515599770.

8. Aure, M.H., Konieczny, S.F., and Ovitt, C.E. (2015). Salivary gland homeostasis is maintained through acinar cell self-duplication. Dev. Cell *33*, 231–237. https://doi.org/10.1016/j.devcel.2015.02.013.

9. Gorgoulis, V., Adams, P.D., Alimonti, A., Bennett, D.C., Bischof, O., Bishop, C., Campisi, J., Collado, M., Evangelou, K., Ferbeyre, G., et al. (2019). Cellular senescence: defining a path forward. Cell *179*, 813–827. https://doi.org/10.1016/j.cell.2019.10.005.

10. Ogrodnik, M. (2021). Cellular aging beyond cellular senescence: markers of senescence prior to cell cycle arrest in vitro and in vivo. Aging Cell *20*, e13338. https://doi.org/10.1111/acel.13338.

11. Robbins, P.D., Jurk, D., Khosla, S., Kirkland, J.L., LeBrasseur, N.K., Miller, J.D., Passos, J.F., Pignolo, R.J., Tchkonia, T., and Niedernhofer, L.J. (2021). Senolytic drugs: reducing senescent cell viability to extend health span. Annu. Rev. Pharmacol. Toxicol. *61*, 779–803. https://doi.org/10.1146/annurev-pharmtox-050120-105018.

12. Nelson, G., Kucheryavenko, O., Wordsworth, J., and von Zglinicki, T. (2018). The senescent bystander effect is caused by ROS-activated NF-kappaB signalling. Mech. Ageing Dev. *170*, 30–36. https://doi.org/10.1016/j.mad.2017.08.005.

13. Biran, A., Perelmutter, M., Gal, H., Burton, D.G.A., Ovadya, Y., Vadai, E., Geiger, T., and Krizhanovsky, V. (2015). Senescent cells communicate via intercellular protein transfer. Genes Dev. *29*, 791–802. https://doi.org/10.1101/gad.259341.115.

14. Dodds, M.W.J., Johnson, D.A., and Yeh, C.K. (2005). Health benefits of saliva: a review. J. Dent. *33*, 223–233. https://doi.org/10.1016/j.jdent.2004.10.009.

15. Aure, M.H., Symonds, J.M., Mays, J.W., and Hoffman, M.P. (2019). Epithelial cell lineage and signaling in murine salivary glands. J. Dent. Res. *98*, 1186–1194. https://doi.org/10.1177/0022034519864592.

16. Delpire, E., and Gagnon, K.B. (2018). Na(+) -K(+) -2Cl(-) cotransporter (NKCC) physiological function in nonpolarized cells and transporting epithelia. Compr. Physiol. *8*, 871–901. https://doi.org/10.1002/cphy.c170018.

17. Kondo, Y., Nakamoto, T., Jaramillo, Y., Choi, S., Catalan, M.A., and Melvin, J.E. (2015). Functional differences in the acinar cells of the murine major salivary glands. J. Dent. Res. *94*, 715–721. https://doi.org/10.1177/0022034515570943.

18. Sneyd, J., Vera-Sigüenza, E., Rugis, J., Pages, N., and Yule, D.I. (2021). Calcium dynamics and water transport in salivary acinar cells. Bull. Math. Biol. *83*, 31. https://doi.org/10.1007/s11538-020-00841-9.

19. Sisto, M., Ribatti, D., and Lisi, S. (2022). E-cadherin signaling in salivary gland development and autoimmunity. J. Clin. Med. *11*, 2241. https://doi.org/10.3390/jcm11082241.

20. Nunnari, J., and Suomalainen, A. (2012). Mitochondria: in sickness and in health. Cell *148*, 1145–1159. https://doi.org/10.1016/j.cell.2012.02.035.

21. Huang, N., Pérez, P., Kato, T., Mikami, Y., Okuda, K., Gilmore, R.C., Conde, C.D., Gasmi, B., Stein, S., Beach, M., et al. (2021). SARS-CoV-2 infection of the oral cavity and saliva. Nat. Med. *27*, 892–903. https://doi.org/10.1038/s41591-021-01296-8.

22. Gervais, E.M., Desantis, K.A., Pagendarm, N., Nelson, D.A., Enger, T., Skarstein, K., Liaaen Jensen, J., and Larsen, M. (2015). Changes in the submandibular salivary gland epithelial cell subpopulations during progression of sjögren's syndrome-like disease in the NOD/ShiLtJ mouse model. Anat. Rec. *298*, 1622–1634. https://doi.org/10.1002/ar.23190.

23. Hsieh, M.-S., Jeng, Y.-M., and Lee, Y.-H. (2019). Mist1: a novel nuclear marker for acinic cell carcinoma of the salivary gland. Virchows Arch. *475*, 617–624. https://doi.org/10.1007/s00428-019-02600-1.

24. Arce-Franco, M., Dominguez-Luis, M., Pec, M.K., Martínez-Gimeno, C., Miranda, P., Alvarez de la Rosa, D., Giraldez, T., García-Verdugo, J.M., Machado, J.D., and Díaz-González, F. (2017). Functional effects of proinflammatory factors present in Sjögren's syndrome salivary microenvironment in an in vitro model of human salivary gland. Sci. Rep. *7*, 11897. https://doi.org/10.1038/s41598-017-12282-x.

25. Jang, S.I., Ong, H.L., Gallo, A., Liu, X., Illei, G., and Alevizos, I. (2015). Establishment of functional acinar-like cultures from human salivary glands. J. Dent. Res. *94*, 304–311. https://doi.org/10.1177/0022034514559251.

26. Saitou, M., Gaylord, E.A., Xu, E., May, A.J., Neznanova, L., Nathan, S., Grawe, A., Chang, J., Ryan, W., Ruhl, S., et al. (2020). Functional specialization of human salivary glands and origins of proteins intrinsic to human saliva. Cell Rep. *33*, 108402. https://doi.org/10.1016/j.celrep.2020.108402.

27. Lin, Y., Cai, Q., Chen, Y., Shi, T., Liu, W., Mao, L., Deng, B., Ying, Z., Gao, Y., Luo, H., et al. (2022). CAFs shape myeloid-derived suppressor cells to promote stemness of intrahepatic cholangiocarcinoma through 5-lipoxygenase. Hepatology *75*, 28–42. https://doi.org/10.1002/hep.32099.

28. López-Otín, C., Blasco, M.A., Partridge, L., Serrano, M., and Kroemer, G. (2023). Hallmarks of aging: an expanding universe. Cell *186*, 243–278. https://doi.org/10.1016/j.cell.2022.11.001.

29. Kühlbrandt, W. (2015). Structure and function of mitochondrial membrane protein complexes. BMC Biol. *13*, 89. https://doi.org/10.1186/s12915-015-0201-x.

30. Sattler, M., Liang, H., Nettesheim, D., Meadows, R.P., Harlan, J.E., Eberstadt, M., Yoon, H.S., Shuker, S.B., Chang, B.S., Minn, A.J., et al. (1997). Structure of Bcl-xL-Bak peptide complex: recognition between regulators of apoptosis. Science *275*, 983–986. https://doi.org/10.1126/science.275.5302.983.

31. Kowaltowski, A.J., Vercesi, A.E., and Fiskum, G. (2000). Bcl-2 prevents mitochondrial permeability transition and cytochrome c release via maintenance of reduced pyridine nucleotides. Cell Death Differ. *7*, 903–910. https://doi.org/10.1038/sj.cdd.4400722.

32. Liu, Y., Sanoff, H.K., Cho, H., Burd, C.E., Torrice, C., Ibrahim, J.G., Thomas, N.E., and Sharpless, N.E. (2009). Expression of p16(INK4a) in peripheral blood T-cells is a biomarker of human aging. Aging Cell *8*, 439–448. https://doi.org/10.1111/j.1474-9726.2009.00489.x.

33. Bettenworth, D., Reuter, S., Hermann, S., Weckesser, M., Kerstiens, L., Stratis, A., Nowacki, T.M., Ross, M., Lenze, F., Edemir, B., et al. (2013). Translational 18F-FDG PET/CT imaging to monitor lesion activity in intestinal inflammation. J. Nucl. Med. *54*, 748–755. https://doi.org/10.2967/jnumed.112.112623.

34. Mabuchi, S., Komura, N., Sasano, T., Shimura, K., Yokoi, E., Kozasa, K., Kuroda, H., Takahashi, R., Kawano, M., Matsumoto, Y., et al. (2020). Pretreatment tumor-related leukocytosis misleads positron emission tomography-computed tomography during lymph node staging in gynecological malignancies. Nat. Commun. *11*, 1364. https://doi.org/10.1038/s41467-020-15186-z.

35. Wati, S.M., Matsumaru, D., and Motohashi, H. (2020). NRF2 pathway activation by KEAP1 inhibition attenuates the manifestation of aging phenotypes in salivary glands. Redox Biol. *36*, 101603. https://doi.org/10.1016/j.redox.2020.101603.

36. Bouma, H.R., Bootsma, H., van Nimwegen, J.F., Haacke, E.A., Spijkervet, F.K., Vissink, A., and Kroese, F.G.M. (2015). Aging and immunopathology in primary sjogren's syndrome. Curr. Aging Sci. *8*, 202–213. https://doi.org/10.2174/1874609808666150727112826.

37. Wick, G., Backovic, A., Rabensteiner, E., Plank, N., Schwentner, C., and Sgonc, R. (2010). The immunology of fibrosis: innate and adaptive responses. Trends Immunol. *31*, 110–119. https://doi.org/10.1016/j.it.2009.12.001.

38. Almássy, J., Siguenza, E., Skaliczki, M., Matesz, K., Sneyd, J., Yule, D.I., and Nánási, P.P. (2018). New saliva secretion model based on the expression of Na(+)-K(+) pump and K(+) channels in the apical membrane of parotid acinar cells. Pflügers Arch. *470*, 613–621. https://doi.org/10.1007/s00424-018-2109-0.

39. Sisto, M., Ribatti, D., and Lisi, S. (2021). Organ fibrosis and autoimmunity: the role of inflammation in TGFbeta-dependent EMT. Biomolecules *11*, 310. https://doi.org/10.3390/biom11020310.

40. Mellas, R.E., Leigh, N.J., Nelson, J.W., McCall, A.D., and Baker, O.J. (2015). Zonula occludens-1, occludin and E-cadherin expression and organization in salivary glands with Sjogren's syndrome. J. Histochem. Cytochem. *63*, 45–56. https://doi.org/10.1369/0022155414555145.

41. Jonckheere, S., Adams, J., De Groote, D., Campbell, K., Berx, G., and Goossens, S. (2022). Epithelial-mesenchymal transition (EMT) as a therapeutic target. Cells Tissues Organs *211*, 157–182. https://doi.org/10.1159/000512218.

42. Sagiv, A., and Krizhanovsky, V. (2013). Immunosurveillance of senescent cells: the bright side of the senescence program. Biogerontology *14*, 617–628. https://doi.org/10.1007/s10522-013-9473-0.

43. Pignolo, R.J., Passos, J.F., Khosla, S., Tchkonia, T., and Kirkland, J.L. (2020). Reducing senescent cell burden in aging and disease. Trends Mol. Med. *26*, 630–638. https://doi.org/10.1016/j.molmed.2020.03.005.

44. Friedman, J.R., and Nunnari, J. (2014). Mitochondrial form and function. Nature *505*, 335–343. https://doi.org/10.1038/nature12985.

45. Green, D.R., Galluzzi, L., and Kroemer, G. (2011). Mitochondria and the autophagy-inflammation-cell death axis in organismal aging. Science *333*, 1109–1112. https://doi.org/10.1126/science.1201940.

46. Correia-Melo, C., Marques, F.D.M., Anderson, R., Hewitt, G., Hewitt, R., Cole, J., Carroll, B.M., Miwa, S., Birch, J., Merz, A., et al. (2016). Mitochondria are required for pro-ageing features of the senescent phenotype. EMBO J. *35*, 724–742. https://doi.org/10.15252/embj.201592862.

47. Tai, H., Wang, Z., Gong, H., Han, X., Zhou, J., Wang, X., Wei, X., Ding, Y., Huang, N., Qin, J., et al. (2017). Autophagy impairment with lysosomal and mitochondrial dysfunction is an important characteristic of oxidative stress-induced senescence. Autophagy *13*, 99–113. https://doi.org/10.1080/15548627.2016.1247143.

48. Cuervo, A.M., Bergamini, E., Brunk, U.T., Dröge, W., Ffrench, M., and Terman, A. (2005). Autophagy and aging: the importance of maintaining "clean" cells. Autophagy *1*, 131–140. https://doi.org/10.4161/auto.1.3.2017.

49. Baker, D.J., Childs, B.G., Durik, M., Wijers, M.E., Sieben, C.J., Zhong, J., Saltness, R.A., Jeganathan, K.B., Verzosa, G.C., Pezeshki, A., et al. (2016). Naturally occurring p16(Ink4a)-positive cells shorten healthy lifespan. Nature *530*, 184–189. https://doi.org/10.1038/nature16932.

50. Acosta, J.C., Banito, A., Wuestefeld, T., Georgilis, A., Janich, P., Morton, J.P., Athineos, D., Kang, T.W., Lasitschka, F., Andrulis, M., et al. (2013). A complex secretory program orchestrated by the inflammasome controls paracrine senescence. Nat. Cell Biol. *15*, 978–990. https://doi.org/10.1038/ncb2784.

51. Herranz, N., Gallage, S., Mellone, M., Wuestefeld, T., Klotz, S., Hanley, C.J., Raguz, S., Acosta, J.C., Innes, A.J., Banito, A., et al. (2015). mTOR regulates MAPKAPK2 translation to control the senescence-associated secretory phenotype. Nat. Cell Biol. *17*, 1205–1217. https://doi.org/10.1038/ncb3225.

52. Yousefzadeh, M.J., Flores, R.R., Zhu, Y., Schmiechen, Z.C., Brooks, R.W., Trussoni, C.E., Cui, Y., Angelini, L., Lee, K.A., McGowan, S.J., et al. (2021). An aged immune system drives senescence and ageing of solid organs. Nature *594*, 100–105. https://doi.org/10.1038/s41586-021-03547-7.

53. Nikolich-Žugich, J. (2018). The twilight of immunity: emerging concepts in aging of the immune system. Nat. Immunol. *19*, 10–19. https://doi.org/10.1038/s41590-017-0006-x.

54. Goronzy, J.J., and Weyand, C.M. (2013). Understanding immunosenescence to improve responses to vaccines. Nat. Immunol. *14*, 428–436. https://doi.org/10.1038/ni.2588.

55. Fülöp, T., Larbi, A., and Pawelec, G. (2013). Human T cell aging and the impact of persistent viral infections. Front. Immunol. *4*, 271. https://doi.org/10.3389/fimmu.2013.00271.

56. He, S., and Sharpless, N.E. (2017). Senescence in health and disease. Cell *169*, 1000–1011. https://doi.org/10.1016/j.cell.2017.05.015.

57. Verstappen, G.M., Gao, L., Pringle, S., Haacke, E.A., van der Vegt, B., Liefers, S.C., Patel, V., Hu, Y., Mukherjee, S., Carman, J., et al. (2021). The transcriptome of paired major and minor salivary gland tissue in patients with primary Sjogren's syndrome. Front. Immunol. *12*, 681941. https://doi.org/10.3389/fimmu.2021.681941.

58. Chen, T., Chen, X., Zhang, S., Zhu, J., Tang, B., Wang, A., Dong, L., Zhang, Z., Yu, C., Sun, Y., et al. (2021). The genome sequence archive family: toward explosive data growth and diverse data types. Dev. Reprod. Biol. *19*, 578–583. https://doi.org/10.1016/j.gpb.2021.08.001.

59. CNCB-NGDC Members and Partners (2021). Database resources of the national genomics data center, China national center for bioinformation in 2022. Nucleic Acids Res. *50*, D27–D38. https://doi.org/10.1093/nar/gkab951.

60. Li, N., Li, Y., Hu, J., Wu, Y., Yang, J., Fan, H., Li, L., Luo, D., Ye, Y., Gao, Y., et al. (2022). A link between mitochondrial dysfunction and the immune microenvironment of salivary glands in primary sjogren's syndrome. Front. Immunol. *13*, 845209. https://doi.org/10.3389/fimmu.2022.845209.

61. Ritchie, M.E., Phipson, B., Wu, D., Hu, Y., Law, C.W., Shi, W., and Smyth, G.K. (2015). Limma powers differential expression analyses for RNA-sequencing and microarray studies. Nucleic Acids Res. *43*, e47. https://doi.org/10.1093/nar/gkv007.

62. Liu, R., Holik, A.Z., Su, S., Jansz, N., Chen, K., Leong, H.S., Blewitt, M.E., Asselin-Labat, M.L., Smyth, G.K., and Ritchie, M.E. (2015). Why weight? Modelling sample and observational level variability improves power in RNA-seq analyses. Nucleic Acids Res. *43*, e97. https://doi.org/10.1093/nar/gkv412.

63. Subramanian, A., Tamayo, P., Mootha, V.K., Mukherjee, S., Ebert, B.L., Gillette, M.A., Paulovich, A., Pomeroy, S.L., Golub, T.R., Lander, E.S., and Mesirov, J.P. (2005). Gene set enrichment analysis: a knowledge-based approach for interpreting genome-wide expression profiles. Proc. Natl. Acad. Sci. USA *102*, 15545–15550. https://doi.org/10.1073/pnas.0506580102.

STAR★METHODS

KEY RESOURCES TABLE

REAGENT or RESOURCE	SOURCE	IDENTIFIER
Antibodies		
Monoclonal Mouse Anti-Human Cytokeratin 7 (for IHC)	Agilent	Cat#GA619; RRID: AB_2925219
Monoclonal Mouse Anti-Human p63	Ibp	Cat#4A4
Anti-VEGF	ZSGB-BIO	Cat#ZM-0265
Polyclonal Rabbit Anti-Human CD3	Agilent	Cat#IR503
Monoclonal Mouse Anti-Human CD8	Agilent	Cat#IR623; RRID: AB_2892113
Monoclonal Mouse Anti-Human CD31	Agilent	Cat#GA610; RRID: AB_2892053
Monoclonal Mouse Anti-Human BCL2	Agilent	Cat#IR614
Monoclonal Rabbit Anti-Human Cytochrome c	Abcam	Cat#ab133504; RRID: AB_2802115
Monoclonal Mouse Anti-Human $p16^{INK4a}$	VENTANA	Cat#06695221001
Monoclonal Mouse Anti-Human p53	Agilent	Cat# GA616; RRID: AB_2889978
Polyclonal Rabbit Anti-Human NKCC1	Proteintech	Cat#13884-1-AP; RRID:A B_2188522
Polyclonal Rabbit Anti-Human Amylase Alpha	Proteintech	Cat#12540-1-AP; RRID: AB_2273990
Polyclonal Rabbit Anti-Human Cytokeratin 7 (for IF)	Proteintech	Cat#17513-1-AP; RRID: AB_2134468
Polyclonal Rabbit Anti-Human E-cadherin	Proteintech	Cat#20874-1-AP; RRID: AB_10697811
Monoclonal Rabbit Anti-Human COX IV	Abcam	Cat#ab202554; RRID: AB_2861351
Polyclonal Rabbit Anti-Human MMP9	Proteintech	Cat#10375-2-AP; RRID: AB_10897178
Monoclonal Mouse Anti-Human CD45	Proteintech	Cat#60287-1-Ig; RRID: AB_2881404
Biological samples		
Human labial salivary glands	Department of Stomatology, Ruijin Hospital, Shanghai Jiao Tong University School of Medicine	N/A
Chemicals, peptides, and recombinant proteins		
sodium succinate	Solarbio	Cat#S8260
Alcian blue (AB)	Servicebio	Cat#G1027
Sirius Red	Sbjbio	Cat#BP-DL030
HE	Provided by department of pathology, Ruijin Hospital, Shanghai Jiao Tong University School of Medicine	N/A
Periodic acid-Schiff (PAS)	Provided by department of pathology, Ruijin Hospital, Shanghai Jiao Tong University School of Medicine	N/A
nitro blue tetrazolium (NBT)	HUSHI	Cat#71029360
NADH Na2	Solarbio	Cat#N8120
DAB	DAKO	Cat#K5007
1× sodium dodecyl sulfate (SDS) buffer	Beyotime	Cat#P0015
TRIzol	Invitrogen	Cat#15596026
Critical commercial assays		
PrimerScript RT Master Mix	Takara Bio	Cat#RR036A
TB Green Premix Ex Taq	Takara Bio	Cat#RR420A

(*Continued on next page*)

Continued

REAGENT or RESOURCE	SOURCE	IDENTIFIER
BOND Polymer Refine Detection kit	Leica	Cat# DS9800
TSA Plus Fluorescein Kit	Servicebio	Cat#G1235-100T
Deposited data		
RNA-sequencing data	This Paper	https://ngdc.cncb.ac.cn/; codes: HRA004187
Experimental models: Organisms/strains		
Female SD Rats	SPF (Beijing) Biotechnology Co., Ltd.	N/A
Oligonucleotides		
Human β-actin forward primer 5′- CATGTACGTTGCTATCC AGGC-3′	BioSune (Shanghai, China)	N/A
Human β-actin reverse primer 5′- CTCCTTAATGTCACGCA CGAT-3′	BioSune	N/A
Human IL-6 forward primer 5′- ACTCACCTCTTCAGAA CGAATTG-3′	BioSune	N/A
Human IL-6 reverse primer 5′- CTCCTTAATGTCACG CACGAT-3′	BioSune	N/A
Human TNF forward primer 5′- GAGGCCAAGCCCTGG TATG-3′	BioSune	N/A
Human TNF reverse primer 5′- CGGGCCGATTGATCT CAGC-3′	BioSune	N/A
Rat gapdh forward primer 5′- CAGGGCTGCCTTCTC TTGTG-3′	BioSune	N/A
Rat gapdh reverse primer 5′- AACTTGCCGTGGGT AGAGTC-3′	BioSune	N/A
Rat IL-6 forward primer 5′-ACAGCCACTGCCTT CCCTA-3′	BioSune	N/A
Rat IL-6 reverse primer 5′- TTGCCATTGCACA ACTCTTT-3′	BioSune	N/A
Rat IL-6β forward primer 5′- GGGATGATGACGA CCTGC-3′	BioSune	N/A
Rat IL-6 reverse primer 5′- AGAATACCACTTG TTGGCTTA-3′	BioSune	N/A
Software and algorithms		
R	Freely available	https://www.r-project.org/
Prism 8	Graphpad-prism	https://www.graphpad.com/

(*Continued on next page*)

Continued

REAGENT or RESOURCE	SOURCE	IDENTIFIER
ggplot2 R package	Freely available	https://cran.r-project.org/web/packages/ggplot2/ggplot2.pdf
ggcor R package v0.9.8.1	Freely available	https://github.com/houyunhuang/ggcor
ImageJ	Freely available	https://imagej.nih.gov/ij/

RESOURCE AVAILABILITY

Lead contact

Further information and requests for resources and reagents should be directed to and will be fulfilled by the lead contact, Liting Jiang (drjiangliting@163.com).

Materials availability

This study did not generate new unique reagents.

Data and code availability

Data reported in this paper will be shared by the lead contact upon request. The raw sequence data reported in this paper have been deposited in the Genome Sequence Archive[58] in National Genomics Data Center,[59] China National Center for Bioinformation/Beijing Institute of Genomics, Chinese Academy of Sciences (GSA-Human: HRA004187) that are publicly accessible at https://ngdc.cncb.ac.cn/gsa-human. This paper does not report original code. Any additional information required to reanalyze the data reported in this paper is available from the lead contact upon request.

EXPERIMENTAL MODEL AND SUBJECT DETAILS

Patients and specimens

Ethics approval of the study was granted by the ethics committee of Ruijin Hospital, Shanghai Jiao Tong University School of Medicine (Shanghai, China). Written informed consent was obtained from all participants before any study procedure. 66 participants were enrolled in this study and stratified into 2 groups: young adults (20–35 years old, female, n = 33) and aged (≥65 years old, female, n = 33), after excluding those with a history of inflammatory, endocrine, or autoimmune diseases. All the tissue samples were collected by labial salivary gland (LSG) biopsies.[60] The biopsy samples were divided into two portions: one portion was used for routine histological analysis (n = 12 per group) and the other portion for molecular analyses (n = 21 per group).

Natural aging rat model

The animal procedures were approved by the Ethics Committee for Animal Care and Use of the Research Center for experimental medicine of Ruijin Hospital, School of Medicine, Shanghai Jiao Tong University, and the Institutional Animal Care and Use Committee of Charles River Laboratories (Shanghai, China). Young (3-month-old, n = 10) and Aged (27-month-old, n = 10) female Sprague-Dawley (SD) rats were subjected to functional salivary gland phenotyping.

METHOD DETAILS

Histological analysis

Samples for histological analysis were fixed in 10% neutral buffered formaldehyde, dehydrated through a graded series of ethanol to xylene, then embedded in paraffin and serially sectioned at 5 μm. Staining with hematoxylin and eosin (HE), periodic acid-Schiff (PAS), and alcian blue (AB)-Sirius red was applied separately to part of the sections according to the standard protocol. Briefly, HE staining was performed by staining rehydrated sections with Mayer's hematoxylin for 6 min, followed by 10 s of staining with eosin. Glycogen was stained purple-red by PAS and the staining procedure is as follows in brief. Rehydrated sections were incubated in periodic acid solution for 10 min then rinsed for 30 s in ddH2O. Then sections were incubated in Schiff's reagent for 20 min followed by washing under running tap water for 5 min. For AB-Sirius red staining, AB highlights acidic glycoproteins blue while Sirius red stains collagen fibers red. Rehydrated sections were stained in Sirius red solution for 1 h, then in AB solution for 15 min, and finally

counterstained in Mayer's hematoxylin for 8 min. Sections were washed under running tap water between each step. All experiments were carried out in a dark and humid container.

The other part of the sections was subjected to immunohistochemical (IHC) staining or immunofluorescence (IF) staining according to the following procedures. Immunostaining was performed on the fully automated Bond-MAX autostaining system (Leica Biosystems, UK). Rehydrated sections were incubated with anti-Bcl-2, anti-CD3, anti-CD8, anti-CD31, anti-CK7, anti-p16, anti-p53, anti-p63, anti-IL-6, anti-TNF-α, anti-cytochrome c and anti-VEGF primary antibodies for 20 min at 25°C after antigen retrieval and blocking. The BOND Polymer Refine Detection kit (DS9800, Leica Biosystems, UK) was used for visualization and counterstaining. The above images were captured using a microscope (Nikon Eclipse Ni-U) equipped with a digital camera (Nikon DS-Ri). IF staining for NKCC1/Amylase, cytokeratin (CK7)/E-cadherin (ECAD), cytochrome *c* oxidase subunit IV (COX IV)/NKCC1 and MMP9/CD45 was carried out on rehydrated sections for co-localization purposes. The staining was amplified with a tyramide signal amplification technique (TSA Plus Fluorescein Kit, Servicebio, China) according to the manufacturer's protocol. Images were taken with a TCS SP8 MP confocal microscope (Leica, Wetzlar, Germany). Antibodies used are listed in the key resources table. All histological analyses and quantifications were performed in a blinded fashion by two independent observers.

Transmission electron microscopy (TEM)

Samples for TEM were pre-fixed in 2.5% glutaraldehyde at 4 °C for 2 h. Then samples were rinsed with PBS for 20 min and post-fixed in 1% osmium tetroxide at 4 °C for 2 h. Dehydration was performed in a graded series of ethanol for 10 min each: 30%, 50%, 70%, 80%, 95%, 2 × 100% (v/v) after washing with ddH2O for 20 min. Then samples were processed using the following propylene oxide (PO) and Epon (Epon 812 resin) series: in pure PO for 20 min; in 1:1 PO/Epon mix for 2 h; in 1:2 mix overnight; and in pure Epon for 6 h. Finally, samples were embedded in pure Epon and polymerized at 60 °C for 48 h. Ultrathin sections (70-90 nm) were prepared by using an EM UC7 ultramicrotome equipped with a diamond knife (Leica, Wetzlar, Germany), mounted on a nickel grid and stained with 3% uranyl acetate and lead citrate. Ultrastructures were investigated with an H-7650 transmission electron microscope (Hitachi, Tokyo, Japan).

Western blot

For glandular tissues, young and aged labial salivary glands (n = 3 per group) were processed for protein extraction. The tissues were homogenated with 1× sodium dodecyl sulfate (SDS) buffer (P0015, Beyotime, Shanghai, China) and boiled at 100°C for 5 min. Proteins were separated by SDS-polyacrylamide gel electrophoresis and electrotransferred to polyvinylidene difluoride(PVDF) membranes (ISEQ00010, Sigma, Darmstadt, Germany), followed by overnight incubation with the primary antibodies (anti-IL-6 and anti-TNF-α at 1:1000 dilution) at 4°C. Active bands were detected using conjugated horseradish peroxidase-conjugated anti-rabbit antibody and anti-mouse antibody (401353,401253, Millipore, Burlington, Massachusetts, USA). Detection was performed by Immobilon Western Chemiluminescent HRP Substrate (WBKLS, Sigma).

RNA extraction and quantitative reverse transcription-PCR (qRT-PCR)

Samples for RNA extraction were stored at −80°C until usage after flash-freezing in liquid nitrogen. Total RNA extraction of each sample was performed using TRIzol reagent (Invitrogen, Carlsbad, CA) according to manufacturer's directions. First-strand cDNA was synthesized using PrimerScript RT Master Mix (RR036A, Takara Bio, Shiga, Japan), and qRT-PCR was performed using TB Green Premix Ex Taq (RR420A, Takara Bio) on a QuantStudioTM 6 Flex Real-Time PCR platform (Thermo Fisher Scientific). β-actin gene was set as the internal control, and each sample was run in triplicate. Melting curve analysis was employed to confirm the specificity of amplification. Relative mRNA expression against β-actin was analyzed using the $2^{-\Delta\Delta Ct}$ method. The primers are listed in the key resources table.

RNA sequencing (RNA-seq) data and gene expression analysis

Tissue samples (n = 13 per group) were disrupted in a motorized homogenizer (Thermo Fisher Scientific Inc., Germany), respectively. Then RNA was extracted using TRIzol Reagent (Qiagen), quantified and qualified using an Agilent 2100 Bioanalyzer (Agilent Technologies, Palo Alto, CA, USA) and a NanoDrop (Thermo Fisher Scientific Inc.). RNA integrity was assessed by gel electrophoresis (1% agarose formaldehyde). The poly(A) RNA was fragmented, reverse transcribed, indexed, amplified, and purified to generate

libraries according to manufacturer instructions. The libraries were multiplexed and loaded on an Illumina Novaseq instrument (Illumina, CA, USA) and run on a 2x 150bp paired-end (PE) configuration. Image analysis and base calling were conducted by the HiSeq Control Software (HCS) + OLB + GAPipeline-1.6 (Illumina) on the HiSeq instrument. Quality control, read mapping and quantification were performed by standard bioinformatic methods. Fold changes were calculated with DESeq2,[61,62] genes with absolute padj<0.05 were considered as differentially expressed. When multiple transcript IDs were present for a gene, the ID with the highest average expression was chosen. For pathway analysis, we use gene Set Enrichment Analysis (GSEA) software at http://www.broad.mit.edu/gsea.[63]

Bioinformatic evaluation and analysis

Quantile normalization and log2 transformation were applied to the raw data before further analysis. Genotype-phenotype correlations using young and aged salivary gland data were calculated by Spearman's rank correlation and visualized using the ggplot2 R package (https://cran.r-project.org/web/packages/ggplot2/ggplot2.pdf). Correlations between SASP and salivary gland microenvironment, including epithelial compartment of salivary glands, immune cell makers, metabolism, and aging related genes (ARGs), were computed with the Mantel test and the Pearson correlation coefficient in young and aged groups. The correlations and their combinations were visualized using the ggcor R package v0.9.8.1 (https://github.com/houyunhuang/ggcor) based on ggplot2.

Animal procedures

After Micro-PET/CT scan, salivary glands were harvested for gene expression analysis and histological study. The qRT-PCR procedures were the same as described above, with the internal control being gapdh. The primers are listed in the key resources table. For histological study, HE staining, AB-Sirius red staining and IF staining of MMP9/CD45 were prepared following the same method as stated above. Samples for succinic dehydrogenase (SDH) and nicotinamide adenine dinucleotide (NADH) staining were instantly immersed in tissue freezing medium (Leica Biosystems, UK) and snap frozen after resection. Cryosections of 5 μm thickness were obtained at −20°C using the CM3050S cryostat (Leica Microsystems, Wetzlar, Germany). For SDH staining, cryosections were incubated with a solution containing sodium succinate, nitro-blue tetrazolium (NBT), and 0.2M phosphate buffer in 37°C water bath for 60 min. Tissue was destained by brief washes in acetone in the following sequence: 30%, 60%, 30% and washed briefly with ddH2O. For NADH staining, the staining solution was prepared by dissolving 1 mg NADH and 1 mg NBT in 1 ml 0.05M Tris-HCl buffer. Sections were incubated with the solution in 37°C water bath for 30 min. Then sections were briefly washed with 60%, 90%, 60% acetone and ddH2O.

Micro-PET/CT scan and image reconstruction

Micro PET/CT imaging was performed on an Inveon MM Platform (Siemens Preclinical Solutions, Knoxville, Tennessee, USA) with a computer-controlled bed and 8.5 cm transaxial and 5.7 cm axial fields of view (FOV). The SD rats were anesthetized with 2% isoflurane in O2 gas for 18F-FDG injection (a single injection of 0.2 ml FDG with an activity of 5 ± 1MBq/100g bodyweight intravenously in the tail vein). 1 hour after administration of the tracer injection, the SD rats were placed prone on the scanner bed and maintained under continuous anesthesia during the study with 1.5% isoflurane in O2 at 2 L/min. Inveon Acquisition Workplace (IAW) 1.5 was used for scanning process. 10 min CT X-ray scanned with a power of 80Kv, 500 uA and an exposure time of 1100 ms before PET scan. 10-minute static PET scans were then acquired, and images were reconstructed by an OSEM3D (Three-Dimensional Ordered Subsets Expectation Maximum) algorithm followed by MAP (Maximization/Maximum a Posteriori) or FastMAP provided by IAW. The 3D regions of interest (ROIs) were drawn over guided by CT images using the software of Inveon Research Workplace (IRW) 4.2.

QUANTIFICATION AND STATISTICAL ANALYSIS

Statistical analysis was conducted with GraphPad Prism. Quantitative result data are presented as means ± standard deviation (SD). Groups were compared using unpaired Student's t-test or one-way ANOVA. Differences were considered statistically significant when P-values < 0.05 (*p < 0.05, **p < 0.01). IHC staining, IF staining, western blot analyses, and qPCR analyses have been repeated at least twice independently.